Ultrasound in Med. & Biol., Vol. 38, No. 7, pp. 1212–1221, 2012

0301-5629/$ - see front matter

ELSEVIER

doi:10.1016/j.ultrasmedbio.2012.01.028

● *Original Contribution*

QUANTITATIVE ULTRASOUND FOR THE MONITORING OF NOVEL MICROBUBBLE AND ULTRASOUND RADIOSENSITIZATION

Justin Lee,[*‡] Raffi Karshafian,[‡§] Naum Papanicolau,[*‡] Anoja Giles,[*†] Michael C. Kolios,[‡§] and Gregory J. Czarnota[*‡]

[*] Department of Radiation Oncology, Odette Cancer Centre, Sunnybrook Health Sciences Centre, and University of Toronto, Toronto, Ontario, Canada; [†] Imaging Research, Sunnybrook Health Sciences Centre, Toronto, Ontario, Canada; [‡] Department of Medical Biophysics, University of Toronto, Toronto, Ontario, Canada; and [§] Department of Physics, Ryerson University, Toronto, Ontario, Canada

(*Received* 8 *September* 2011; *revised* 23 *January* 2012; *in final form* 27 *January* 2012)

Abstract—There is a need for cancer imaging to provide "real-time" information about the metabolic and cellular responses of tumours. Quantitative ultrasound techniques have recently been demonstrated to be a potential method of assessing tumour response at the cellular level. Anti-cancer treatments administered to xenograft-bearing mice consisted of radiotherapy and a novel antivascular therapy utilizing encapsulated microbubble agents in the presence of ultrasound. Radiation dose and microbubble concentrations were varied and the treatment modalities were given in combination to assess the possible enhancement of tumour cell death. Quantitative methods were used to non-invasively assess responses. Results demonstrated statistically significant changes in backscatter parameters (midband fit, spectral intercept) in tumours treated with high doses of radiotherapy or a high concentration of microbubbles. Combined treatments demonstrated further increases in ultrasound parameters. Histopathologic assessment was used and tumour cell death was found to correlate with increases in ultrasound parameters. (E-mail: Gregory.Czarnota@sunnybrook.ca) **© 2012 World Federation for Ultrasound in Medicine & Biology.**

Key Words: **Quantitative ultrasound, Cell death, Microbubble, Antivascular therapy, Radiation.**

INTRODUCTION

Tumour response imaging

The accurate and predictive medical imaging of tumour response during the course of treatment has the potential to shift the paradigm in oncology from predetermined treatment regimens toward individualized and adaptive treatment pathways based on tumour response "biomarkers" and early assessments of tumour response (reviewed in Brindle 2008). With an increasing number of cancer therapeutics available including targeted antibodies, antivascular agents, chemotherapy and radiation, there is an increasing need for more personalized treatments to optimize efficacy while avoiding excessive and unnecessary toxicity. It may be possible, given recent advances in methods, to use new quantitative ultrasound imaging techniques to personalize therapy.

Common imaging modalities used to image tumour response currently include X-rays, computed tomography and magnetic resonance imaging. Tumour size and volume are measured but may take weeks to months after the commencement of treatment to demonstrate response. Positron emission tomography and magnetic resonance spectroscopy can often be used to demonstrate metabolic responses at an earlier time (Brindle 2008) but remain costly at this time and are not widely available. Ultrasound represents an alternative noninvasive, inexpensive, imaging modality that has the potential to detect early tumour response linked to changes occurring at the cellular level during the course of cancer treatment.

High frequency ultrasound can be used to detect tumour cell changes associated with cell death, such as DNA condensation and fragmentation caused by cancer treatments (Czarnota et al. 1999). Scattering properties of the tumour including acoustic scatterer size, acoustic concentration, impedance and spatial organization can be affected by anti-cancer treatments and subsequently result in increases in ultrasound image intensity (Hunt et al. 2002; Kolios et al. 2002; Taggart et al. 2007). These changes can be quantified through the analysis of radio-frequency (RF) spectral data that is received by all ultrasound devices prior to translation to a clinical

Address correspondence to: Gregory J. Czarnota, M.D., M.Sc., F.R.C.P.C., Department of Radiation Oncology, Sunnybrook Health Sciences Centre, 2075 Bayview Avenue, Suite T2-167, Toronto, ON, M4N 3M5, Canada. E-mail: Gregory.Czarnota@sunnybrook.ca

image. These principles have been demonstrated in multiple tumour types and varying therapeutic modalities (reviewed in Czarnota and Kolios 2010).

For example, early work *in vitro* by Czarnota et al. (1997, 1999) utilized highly controlled models of acute myelogenous leukemia (AML) cells treated with cisplatinum to induce apoptosis and separately colchicine and enzymes to study the effects of nuclear condensation. These experiments established that high frequency ultrasound backscatter can increase by nearly 12 dBr (decibels, normalized to a standard quartz reference) with apoptotic cell death and nuclear condensation. In addition, an increase in the spectral slope parameter was associated with a decrease in nuclear size, which corresponded closely with theoretically predicted values (Kolios et al. 2002). Vlad et al. (2005) examined *ex vivo* liver specimens with ultrasound to assess ischemic changes causing cell death and found backscatter increases in the range of 4–9 dBr. Another *ex vivo* study reported by Oelze et al. (2004) examined mammary tumours with 8.5 MHz ultrasound immediately after euthanizing the animals. In that study, RF analysis was used to differentiate benign mammary fibroadenomas from breast cancer xenografts based on the scatterer size and acoustic concentration of specimens. Similar ultrasound tissue characterization techniques have been used to evaluate and differentiate structures within the eye, prostate gland and kidney (Lizzi et al. 1997, 2006).

Noninvasive ultrasound-based tumour response imaging *in vivo* is a relatively recent development. The first preclinical application of quantitative ultrasound to monitor tumour response was reported by Banihashemi et al. (2008) who evaluated malignant melanoma tumours in mice prior to and after photodynamic therapy. Ultrasound backscatter parameters correlated with cell death; peak ultrasound intensity was observed 24 hours after treatment when maximal cell damage was evident. A similar *in vivo* study by Vlad et al. (2009) studied head and neck carcinoma xenografts before and after radiotherapy treatments. The tumours exhibited an increase of integrated ultrasound backscatter of up to 8.2 dB 24 h after radiotherapy and large hyperechoic regions corresponding to histologic areas of cell death were seen; the spectral slope parameter also increased after radiotherapy. Here, for the first time, we use high frequency ultrasound in a similar manner, to monitor *in vivo* tumour responses to novel vascular disrupting combined radiotherapy and microbubble-based treatments.

Ultrasound and microbubble enhancement of radiation treatment

Radiation therapy causes tumour cell death through a complex process of free radical production and DNA strand breaks, resulting in mitotic catastrophe and other forms of cell death. Current radiobiology research also suggests that alterations of the tumour stroma, microenvironment and microvasculature are closely linked to radiation response. Garcia-Barros et al. (2003) demonstrated that for high single-fraction doses of radiotherapy, endothelial cell death and ceramide pathway activation was a requisite for tumour cell death, whereas with low doses, this was inhibited by hypoxia-inducible factor. In addition, antivascular and anti-VEGF agents are being evaluated presently by others in conjunction with radiation in an attempt to exploit this dependence on the microvasculature (Nieder et al. 2006).

Microbubbles have been used successfully as diagnostic ultrasound contrast agents for cardiac and hepatic imaging because they reflect a characteristic echo due to nonlinear oscillation that can be detected using harmonic imaging (Lanka et al. 2007; Mulvagh et al. 2008). Their size and composition permits them to persist exclusively in the circulation and the microvasculature after intravenous injection. Recent observed bioeffects of microbubbles and ultrasound such as transient membrane permeabilization, microvascular leakage and endothelial cell death have stemmed interest in potential therapeutic applications using microbubbles such as gene therapy, localized drug delivery and thrombolysis (Unger et al. 2002). In the experiments here, microbubbles were utilized in combination with radiation, to enhance tumour response. The detailed biologic and molecular mechanisms underlying this novel technique of utilizing microbubbles to target the microvasculature is described in other work (Al-Mahrouki et al. 2010).

The purpose of the current study was to use high frequency ultrasound to detect early cell death caused by radiation and the novel use of ultrasound and microbubbles as radio-enhancing antivascular agents. This is a novel therapeutic approach that targets the tumour by directing the known bioeffects of microbubble agents toward a small region defined by a focused ultrasound beam. Ultrasound treatment was then combined with radiotherapy to treat prostate cancer xenografts *in vivo* to evaluate the potential enhancement of tumour cell death. Then, using quantitative high frequency ultrasound imaging, similar to that described in previous studies, evaluations of tumour responses after treatment were carried out. Ultrasound spectroscopic results were also compared with histopathologic specimens. We found an independent effect of ultrasound and microbubble treatments as a singular modality and, when combined with radiotherapy, there was also an enhancement of overall tumour cell death. Further, we found in this study that morphologic changes and cell death induced by the two treatments could be detected *in vivo* using quantitative high frequency ultrasound.

MATERIALS AND METHODS

Tumour growth

Severe combined immuno-deficient (SCID) mice bearing a human prostate cancer cell line (PC-3, ATCC 1435) as xenografted tumours were utilized in this study ($n = 49$). Tumour cells were actively grown in culture and an intra-dermal injection of 10^6 tumour cells within a 50 uL volume was administered into the right hind leg of each SCID mouse to establish tumours. Tumours were grown to a size of 7 to 8 mm in maximum diameter over approximately 4–6 weeks. Mice were anaesthetized using a mixture consisting of ketamine 100 mg/kg, xylazine 5 mg/kg and acepromazine 1 mg/kg administered by IP injection of 0.1 mL per animal for imaging and treatment. Animals were handled in accordance with institutional animal care policies.

High frequency ultrasound imaging

All animals underwent high frequency ultrasound imaging prior to treatment, using a VS40-B ultrasound device (Visualsonics, Toronto, Canada), which is capable of recording standard B-scans as well as raw RF data. Imaging and data collection was repeated 24 h after treatment, which has been demonstrated in previous studies to be the time potentially most sensitive to early death effects detectable in the ultrasound backscatter spectrum (Banihashemi et al. 2008; Czarnota et al. 1999). A 30 MHz transducer was utilized (F2-30-03) with an f-number of 2.13, a focal depth of 12.8 mm, a 90% bandwidth pulsed at centre frequency of 25 MHz. The depth of field of the transducer was 1.72 mm, with a lateral resolution of 149 μm and an axial resolution of 54 μm. Animals were secured on a plastic stage with the hind leg and tumour immersed in degassed water. The transducer was consistently positioned such that the focus was located 2–2.5 mm into tumour from the tumour surface. Beginning from the upper leg, the transducer was moved toward the foot by a motorized micropositioning system that utilizes a two-dimensional (2-D) raster scanning pattern to provide multiple, parallel, cross-sectional images of the tumour. Images were acquired 0.4 mm apart with an average of 10–20 images per tumour. RF data was acquired using a sampling frequency of 500 MHz, with 30 independent RF lines per image and 2870 samples per RF line.

Treatment groups

Animals were administered one of nine possible treatments: no treatment, radiotherapy alone (2 Gy or 8 Gy given in a single fraction), ultrasound in the presence of microbubbles alone (low or high concentration, 1% or 3% of blood volume, respectively), or a combined treatment with radiotherapy given immediately after ultrasound and microbubbles. Animals were also treated with ultrasound alone and microbubbles alone to control for independent effects of these modalities. Animals were euthanized by cervical dislocation under anaesthesia after 24 h, for the assessment of acute morphologic changes by pathology. Animals were handled following guidelines of the Animal Care Council of Canada.

High frequency ultrasound spectral analysis

A VS40-B ultrasound device was used to digitally record all images and RF data. A region-of-interest (ROI) was chosen within the tumour measuring approximately 3×3 mm centred at the focal depth. The ROI was selected consistently to exclude the skin and to minimize the thickness of the intervening tumour tissue between the skin and the ROI. Attenuation coefficients for the skin was assumed to be 0.2 dB/mm/MHz (Shung 2005). The thickness of the skin was previously measured from ultrasound images in similar *in vivo* mouse models, yielding values of 0.30 ± 0.06 mm for untreated tumours and 0.45 ± 0.15 mm for irradiated tumors (Vlad et al. 2009). The thickness of the intervening tissue between the skin and ROI was 0.4 ± 0.20 mm. The attenuation coefficient of the intervening tumor tissue was estimated to be 0.06 dB/mm/MHz based on previous *in vivo* and *in vitro* studies that included measurements both prior to and 24 h after irradiation (Vlad et al. 2008, 2009). Between 10 to 15 ROIs were sampled per animal and averaged for spectral analysis. Three previously established RF parameters were evaluated prior to and 24 h after treatment to monitor response to ultrasound activated microbubbles and radiotherapy: spectral slope (SS), midband fit (MBF) and 0-MHz intercept (0-MHz). These parameters have previously been demonstrated to be related to tumour cell characteristics associated with apoptosis (Banihashemi et al. 2008; reviewed in Czarnota and Kolios 2010). Spectral analysis results were then compared with a quantification of histopathology at low and high magnification.

Microbubble injections and low frequency activating ultrasound

Lipid-encapsulated perfluoropropane microbubbles (Definity, Perflutren lipid microspheres; Lantheus Medical Imaging, Billerica, MA, USA) were injected *via* tail vein catheter. The agent was activated prior to use using a mechanical shaking device for 45 s at 3000 rpm. Two microbubble concentrations were employed for treatments: high (3% v/v) and low (1% v/v). For 3% (v/v) concentration, 150 uL of microbubbles was added to 100 uL of normal saline to form an injectable dilution. 100 uL single bolus injection of the dilution was administered over 30–60 s, followed by 150 uL normal saline to flush the tail vein catheter. The estimated number of

bubbles per millilitre (mL) of blood was 2.4×10^9. The 1% microbubble concentration was similarly achieved with 100 uL bolus injection of 100 uL with 400 uL normal saline dilution. The mice were then secured to a staging set-up with the lower half of the mouse and the tumour immersed in a tank of degassed water, maintained at a temperature of 37°C. The staging system was positioned with the tumour centered within the focus of the ultrasound beam. The low frequency "bubble-activating" treatment ultrasound was generated using a 500 kHz focused transducer (IL0509HP; Valpey Fisher Inc., Hopkinton, MA, USA) with a diameter of 2.87 cm, focal depth of 8.5 cm, a peak negative pressure of 570 kPA, a –6 dB beam width of 31 mm and depth of field greater than 2 cm. The transducer was connected to a waveform generator AWG520; (Tektronix Inc., Beaverton, OR, USA), a power amplifier and receiver (RPR4000; Ritec Inc., Warwick, RI, USA) and a PC-controlled digital acquisition system (Acquiris CC103; Agilent Technologies Inc., Monroe, NY, USA) using the set-up described previously by Karshafian et al. (2009). Ultrasound consisted of tone bursts, with a duration of 32 us (16 cycles) each, and a pulse repetition frequency of 3 kHz, over 50 ms. Each 50 ms sonication was followed by 1950 ms of no ultrasound. The treatment was administered over a total time of 5 minutes, resulting in an overall duty cycle of 0.24% (or 720 ms of treatment time with the beam on) designed to avoid ultrasound heating biologic effects. The transducer I_{SPTP} was 22.4 W/cm^2 and the I_{SPTA} was 0.054 W/cm^2. Spatial peak temporal average (SPTA) intensity was calculated by multiplying spatial peak temporal peak (SPTP) intensity by the time duration that ultrasound is on (720 ms) divided by the total treatment duration (300 s). A micropositioning system was used to center the tumour within the focus of the ultrasound; the –3 dB beam width was determined to be 15.6 mm to ensure that the entire tumour (average diameter 8 mm) was exposed to the ultrasound pulse in a reproducible fashion.

Radiation

Animals receiving radiation were treated with a 160 kVp small animal X-ray irradiator (Faxitron Cabinet X-ray System; Faxitron X-ray Corporation, Toronto, ON, Canada) at a rate of 200 cGy/min. A lead cutout was placed to shield the animal and irradiate only the tumour. Single fraction doses of 2 or 8 Gy were administered immediately following ultrasound treatments.

Histopathology

Tumours were excised immediately following the 24 h "post-treatment" scan, fixed in 10% neutral–buffered formalin for 12 h, embedded in paraffin then sectioned in the approximate imaging plane and stained with standard hematoxylin and eosin (H&E). To assess apoptotic cell death, the *in situ* end-labelling (ISEL) assay was performed. High magnification images were acquired using a LEICA DMLB light microscope coupled to a digital camera (Leica DC200, Leica Microsystems, Wetzlar, Germany) to permit quantitative analysis. Image J software (NIH, Bethesda, MA, USA) was used to estimate total tumour area and gross apoptotic or necrotic areas from H&E and ISEL stained images (Rasband 1997). The visible region of ISEL positive staining was calculated as a percentage of the total tumour cross section area and one to two slides per animal were averaged for a minimum of four animals per group. Within high magnification ISEL specimens, open-source image analysis cell profiler software (Version 1.0; Broad Institute, Cambridge, MA, USA) was used for quantification of cell death and to estimate nuclear size (Carpenter et al. 2006). For each tumour sample, the data were collected from three different regions of the treated area and averaged during analysis (minimum 12 ROIs for each treatment condition).

Statistical methods

The paired *t*-test was employed within each treatment group to assess changes in spectral parameters measured at baseline and 24 h later. A two-way factorial analysis of variance (ANOVA) was utilized to determine whether microbubble treatments and/or radiation treatment had an effect on ultrasound measurements and the Holm-Bonferroni correction was applied for multiple tests. The Pearson correlation was calculated to assess agreement between histopathology and spectral parameters. Origin Pro software (Version 8.1; OriginLab Corporation, Northampton, MA, USA) was used for statistical analysis.

RESULTS

HFUS spectral analysis

Before and at 24 h after treatment, images and backscattered ultrasound data were collected for each mouse. Ultrasound and microbubble treatment combined with radiotherapy produced constant and reproducible changes in ultrasound images and spectral variables of midband fit and 0-MHz intercept.

The midband fit of the tumours was -49.3 ± 0.3 dBr prior to treatment whereas 24 h after treatment, significant increases in the midband fit parameter were observed in tumour groups treated with 8 Gy alone, 3% microbubbles and ultrasound alone and all combinations involving 8 Gy or 3% microbubbles and ultrasound. The greatest increase was observed after combined 8 Gy with 3% bubble and ultrasound treatments. This was an increase of 5.2 ± 1.4 dBr (from -51.3 to -46.1, $p = 0.014$), which represents a greater than three-fold increase in ultrasound backscatter intensity (Figs. 1 and 2). A two-way factorial

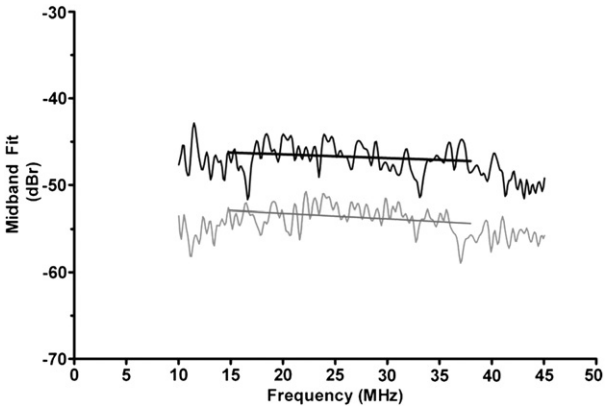

Fig. 1. Quantitative ultrasound data. Representative high frequency quantitative ultrasound backscatter analyses with best fit lines plotted over the −6 dB bandwidth. Note the change in the midband fit and 0-MHz intercept between pretreatment (gray lines) and post-treatment (dark lines) samples. Scans are averages of data from 10 fields of view from a representative tumour.

ANOVA demonstrated a main effect of radiation dose, $F(2,38) = 10.63$, $p < 0.001$, indicating tumours treated with radiation alone had a statistically significant higher midband fit. A main effect of microbubble concentration was also detected with $F(2,38) = 9.75$, $p < 0.001$. There was a moderate, statistically significant positive correlation between midband fit and aggregate tumour cell death ($r = 0.46$, $p = 0.001$) as assessed from histologic sections of treated tumours.

The 0-MHz intercept parameter increased by a maximum of 6.3 ± 1.9 dBr (from −48.5 to −42.2, $p = 0.021$) after combined treatment with 8 Gy and 3% microbubbles and ultrasound. Statistically significant but lesser increases were seen in tumours treated with 8 Gy alone, 3% bubbles and ultrasound alone and all combined treatment groups (Fig. 2). A two-way factorial ANOVA demonstrated main effects of both radiation, $F(2,38) = 9.823$, $p < 0.001$ and microbubble treatments, $F(2, 38) = 6.13$, $p = 0.005$ on the 0-MHz intercept parameter. Correlation between the 0-MHz intercept and aggregate cell death was moderate ($r = 0.42$, $p = 0.003$).

The spectral slope parameter did not change between scans conducted before and after 24 h for any treatment group. In addition, an ANOVA did not show any main effects of radiation or microbubbles and the correlation coefficient between spectral slope and cell death was nearing zero ($r = -0.002$, $p = 0.99$). Data are presented parametrically with colour overlays in Fig. 3.

Qualitative histopathologic results

Standard hematoxylin and eosin (H&E) staining of the tumour specimens demonstrated expected results with single fraction radiation treatment using 2 Gy: there were no obvious regions of cell death and tumour cells

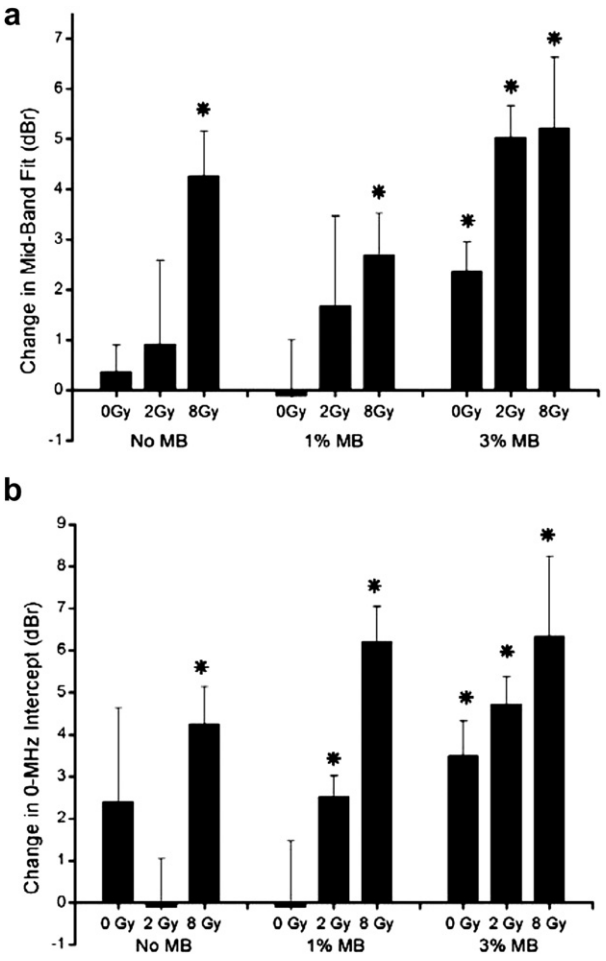

Fig. 2. (a) Treatment condition vs. change in midband fit. Increases in midband fit are normalized to a quartz reference (and given in dBr). Error bars represent standard error of the mean; the asterisk (*) signifies statistically significant result by paired *t*-test, $p < 0.05$, Holm-Bonferroni correction for multiple tests. (b) Treatment condition vs. change in 0-MHz Intercept. The 0-MHz intercept is given in dBr. Error bars represent standard error of the mean; the asterisk (*) signifies statistically significant result by paired *t*-test, $p < 0.05$, Holm-Bonferroni correction for multiple tests.

were homogeneous and tightly packed. With the 8 Gy specimens, 24 h after treatment, there were sparse, small regions of decreased apparent cell density, suggesting cell death and necrosis. In contrast, ultrasound and microbubble treatments caused a heterogeneous appearance consisting of larger confluent patches of apparent cell death that stained poorly with H&E, surrounded by viable, healthy looking cells at the periphery of the tumour. The size and number of regions of cell death increased with higher microbubble concentration. Tumours treated with combined microbubbles and ultrasound and radiation demonstrated the largest confluent patches tumour cell disruption and death (Fig. 4).

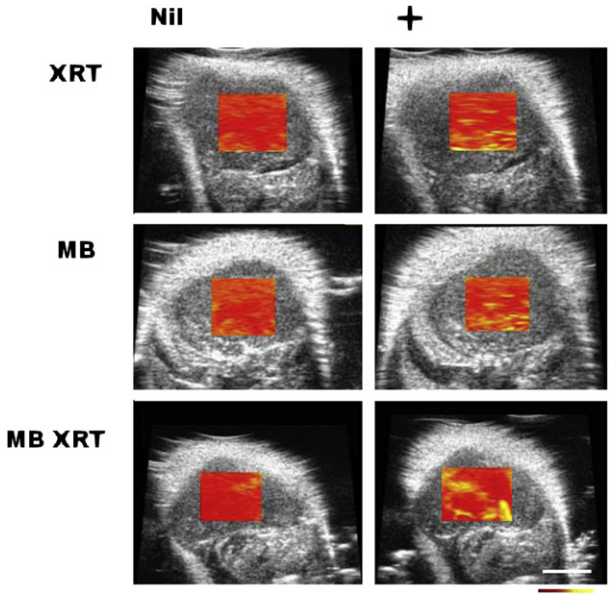

Fig. 3. Representative parametric images of treatment effects. Nil column indicates data before treatment, + column indicates data 24 h after treatment, radiotherapy alone (XRT) indicates 8 Gy radiation, microbubble (MB) indicates treatment with ultrasound-stimulated microbubbles and MB XRT indicates combined treatment. The scale bar represents 3 mm. The colour map indicates a change of 6 dB from red to yellow.

At higher magnification, changes associated with 8 Gy included cellular condensation, apoptotic nuclear fragmentation and primarily nuclear coalescence secondary to mitotic arrest/catastrophe. With microbubble and ultrasound treatment alone, the predominant mode of cell death appeared to be consistent with ischemic apo-necrosis, characterized by cellular and nuclear debris, cytoplasmic changes and cellular degradation. For combined treatment, apoptotic and necrotic changes were present.

Quantitative histopathologic results

Quantitative analysis of ISEL stained sections demonstrated minimal tumour cell death with treatment with 2 Gy and 8 Gy radiation doses as compared with untreated controls. The mean area of tumour cell death comprised 3 ± 3% of the total tumour area with 2 Gy radiation treatments and 9 ± 13% for tumours receiving 8 Gy of radiation (Fig. 5). Ultrasound combined with microbubble agents alone as a treatment caused significant cell death centrally within the tumours, which increased with higher concentrations; up to 34 ± 13% cell death as a proportion of total tumour area. Maximal regions of ISEL positive cell death were achieved with combined high dose radiation and high concentrations of bubbles (63 ± 5%). Ultrasound treatments without microbubbles were equivalent to untreated controls.

Quantification of high magnification histopathology demonstrated increased cell death with the addition of microbubbles and ultrasound to radiotherapy, corresponding to regions of dense staining of both prostate tumour cells and debris, likely representing endothelial cells, DNA fragmentation and leakage. The number of ISEL positive stained cells per high power field was low in the untreated group, as expected (1 cell per high power field), and also low in the radiotherapy alone groups; 48 ± 32 and 28 ± 40 cells per field for 2 Gy and 8 Gy, respectively. Cell death increased with the addition of microbubble treatments, reaching a plateau in the combined 2 Gy with ultrasound and bubbles (172 ± 57 cells per high power field) and 8 Gy with ultrasound/bubbles groups (171 ± 78 cells per high power field) (Fig. 5).

DISCUSSION

As the breadth of treatment options available to patients and health care providers increases, the need for accurate, simple and predictive imaging to monitor and help guide therapy will necessarily follow. New methods of imaging tumour response will potentially guide appropriate and personalized therapeutics. The current study confirms that ultrasound spectroscopy can detect tumour cell death *in vivo*. Utilizing a prostate cancer model, high frequency ultrasound was able to detect tumour cell death caused by radiation and microbubble-induced antivascular treatments independently and also, for the first time, a novel combined treatment modality effect.

In multiple previous *in vitro* and *in vivo* studies, where apoptosis was a predominant mode of cell death, the observed increases in ultrasound integrated backscatter or the midband fit parameter varied between 6.5 dBr to 13 dBr (Kolios et al. 2002; Vlad et al. 2009). For the study here, the amplitude of changes in midband fit were lower but reproducible and statistically significant, in the range of 4 dBr to 6 dBr. This difference was likely reflective of the various modes of cell death induced within this *in vivo* model, with not only endothelial cell apoptosis, but also secondary tumour cell death. The Pearson's correlation between histopathologic results and changes in midband fit or 0-MHz intercept parameters yielded only moderate correlations ($r = 0.46$ and $r = 0.42$, respectively), suggesting more complexity in the factors affecting ultrasound backscatter beyond the direct quantification of regions of tumour cell death. Changes in ultrasound spectroscopy for any application will be highly dependent on the tumour biology, treatment modality and the surrounding microenvironment. We have previously detected comparable increase of backscatter with mixed forms of cell death (Vlad et al. 2009).

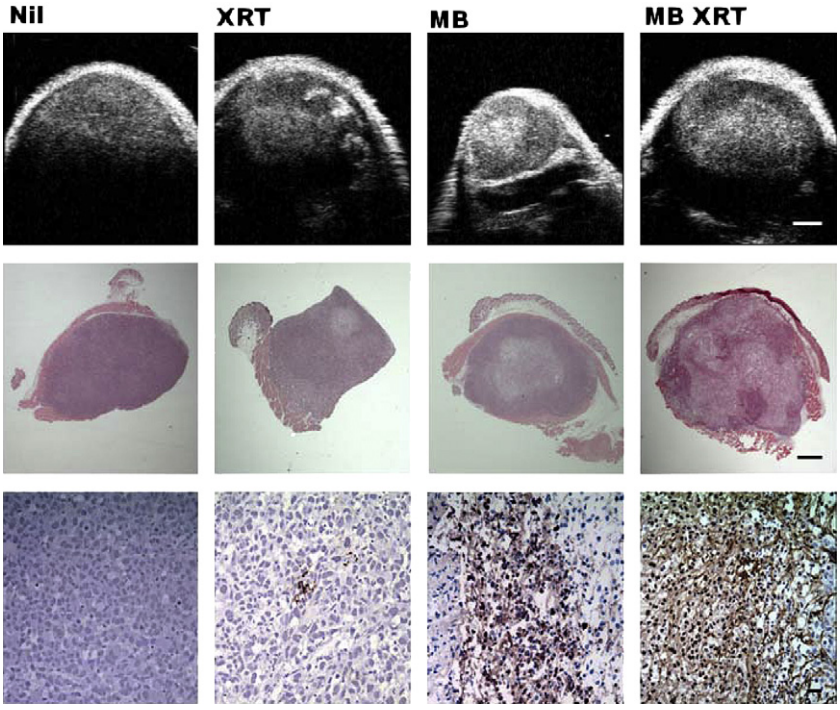

Fig. 4. Representative images of ultrasound B-scans, low magnification haematoxylin and eosin (H&E) microscopy and high magnification *in situ* end-labelling (ISEL) stained specimens. The top row presents high-frequency ultrasound images of tumours (sale bar represents 1 mm). The second row H&E stained slides (scale bar represents 1 mm) and the third *in situ* end-nick labelled specimens (the scale bar represents 20 μm). The first column in an untreated control specimen (Nil) both the B-scan and low magnification images have a uniform, homogeneous appearance within the tumour and no brown ISEL staining is present. The second column, treated with 8 Gy radiotherapy alone (XRT) demonstrated small hyperechoic regions on B-scan and heterogeneous regions within the H&E specimen; at higher magnification some ISEL staining is detected in a limited number of cells. High concentration microbubble treatments (MB, third column) caused a large centralized region of cell death with a mixed picture of ISEL stained cells and necrosis at high magnification. When combined treatments were applied (far right column, MB XRT), there was heterogeneity within the tumour B-scan and an irregular appearance on H&E with extensive cell death; corresponding to regions of very dense ISEL staining at high magnification. ISEL positive regions corresponded to regions of pallor in H&E staining macroscopically.

The relative radiosensitivity and predominant forms of cell death in tumours vary greatly with the type of cell irradiated. Lymphoid and myeloid cells, for example, are highly sensitive to radiotherapy, and a large proportion undergo apoptosis 3 to 6 h after irradiation. Leukemia cells treated with 10 Gy have demonstrated apoptosis beginning at 6 h and the percentage of apoptotic cells increased steadily with time, plateauing at approximately 35% apoptotic cells at 24 h (Verheij and Bartelink 2000). In contrast, human prostate cancer cell lines appear to undergo cell death predominantly by mechanisms of mitotic catastrophe or terminal growth arrest (senescence) rather than apoptosis. To determine the role of apoptosis in irradiation of prostate cell lines, Bromfield et al. (2003) used nuclear morphologic features, the presence of apoptotic bodies and associated protein expression to quantify radiation-induced apoptosis in relation to overall clonogenic cell kill. For prostate cancer cell lines, including PC-3, which was used in the current study, the apoptotic response was low (0%–6% of cells) and not dose-dependent up to 20 Gy. Experiments *in vitro* were also supported by minimal TUNEL staining of irradiated PC-3 tumours by the same investigators who noted a "senescence-like phenotype" that appeared to be associated with cell granularity as measured by increased side scatter coefficient using fluorescent flow cytometry. In this study, we also treated PC-3 tumours with single fractions of radiotherapy and found a similarly low ratio of apoptotic cells by histology and immuno-histochemistry. Despite limited areas of ISEL-associated DNA strand breaks and apoptosis, the midband fit and 0-MHz intercept parameters still increased significantly with 8 Gy radiotherapy. This supports the idea that forms of cell death or damage other than apoptosis (such as a senescence-like phenotype with mitotic-arrest) can also alter cell morphology and result in ultrasound backscatter changes as previously demonstrated (Vlad et al. 2009).

From treatment groups of ultrasound and microbubbles only, the predominant mode of cell death with this novel therapeutic approach appeared to be ischemic

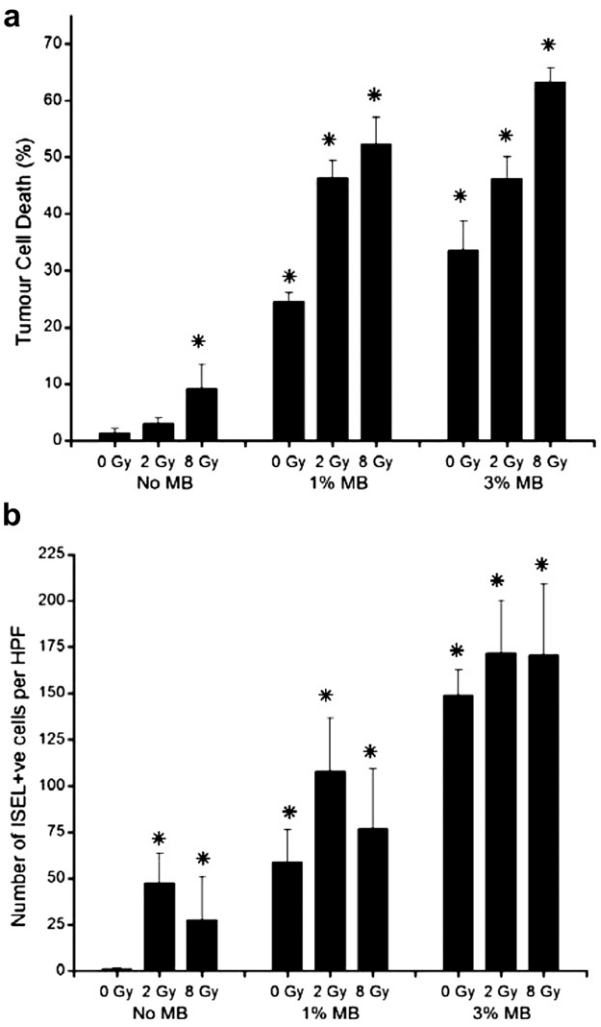

Fig. 5. (a) Treatment condition vs. tumour cell death (% area). Bars show percent area of tumour cell death quantified by low magnification haematoxylin and eosin (H&E) and *in situ* end-labelling (ISEL) analysis. Error bars signify inter-tumour variation and represent the standard error of the mean. The asterisk, (*) signifies statistically significant result by unpaired Student's *t*-test, $p < 0.05$, compared with untreated controls. (b) Treatment condition vs. number of ISEL positive cells per HPF. Bars show the density of tumour cell death within regions-of-interest at high magnification by analysis of ISEL stained tumour sections. Error bars signify inter-tumour variation and represent the standard error of the mean. The asterisk (*) signifies statistically significant result by unpaired Student's *t*-test, $p < 0.05$, compared with untreated controls.

necrosis. Low-magnification specimens demonstrated well demarcated regions of cell death, with weak staining consistent with necrosis and phagocytosis of cell remnants. At higher magnification, classic features of necrosis such as cellular debris and fragments were observed. Therefore, when combined with radiotherapy, the overall treatment effects could be expected to include mitotic arrest and catastrophe, senescence, apoptosis and necrosis. Features of ischemic necrosis may account for spectroscopic changes of lesser magnitude than in previous *in vivo* studies as seen in Banihashemi et al. (2008) with cellular disintegration. Another previous study of ischemic and necrotic liver tissue yielded an average increase in ultrasound integrated backscatter of 6 dBr and a range of 4–9 dBr, which is closer to the changes observed in this study here (Vlad et al. 2005, 2009). In a separate study of cells undergoing necrosis *in vitro,* a decrease in the midband fit parameter was demonstrated (Ranieri et al. 2008) indicating the possibility of moderating or counterbalancing increased backscatter induced by apoptosis. The use of ultrasound and microbubble treatments has the potential to introduce additional sources of scattering such as endothelial cell apoptosis, and intermediaries of apoptosis and necrosis.

The spectral slope parameter is most closely associated with average scatterer size based on theory and demonstrated by *in vitro* studies. For example, using polystyrene spheres in agarose gel, Bridal et al. (1996) used ultrasound backscatter parameters to accurately estimate the size of scatterers as small as 5.1 μm, approximately one sixth of the 25 MHz transducer wavelength. Other researchers have also determined the size of subwavelength scatterers using spheres in suspension or single cells (Bigelow et al. 2005; Kolios et al. 2002). With increasingly complex models such as cell pellets or tumours *in vivo*, spectral slope analysis has produced varying results. Kolios et al. (2002) studied AML cells treated with apoptosis-inducing chemotherapy and found that increasing spectral slope did correlate with a relative decrease in nuclear size, but in terms of absolute values, the model overestimated the true nuclear size by a factor of 3.5. When AML cells were irradiated, no significant change in spectral slope was observed and histopathologic specimens demonstrated a mixed response with small apoptotic fragments and condensed nuclei as well as enlarged cells undergoing mitotic catastrophe (Vlad et al. 2008). Head and neck cancer cell lines (FaDu and Hep-2) treated with radiotherapy *in vitro* exhibited mitotic catastrophe/arrest and ultrasound analysis demonstrated a decrease in the spectral slope parameter associated with an enlarged nuclear size. In contrast, when the same cell lines were grown as xenografts in immunodeficient mice, spectral slope increased with the FaDu tumours while Hep-2 tumours could not be assessed due to radioresistance *in vivo* (Vlad et al. 2009). In the experiments here, using PC-3 prostate cancer cells, spectral slope was invariant amongst all treatment groups. Post hoc analysis of nuclear and fragment size using image analysis software demonstrated increasing variance but near constant average size; a similar result was observed by Banihashemi et al. (2008) where midband fit and

0-MHz intercept increased with no change in the spectral slope. Randomization of scatterers could also potentially cause increases in the other two parameters without influencing the spectral slope. Hunt et al. (2002) showed that increasing variance in cell size and randomization of microstructure positioning can increase backscatter even without changes in individual scatterer properties.

The combined treatments in this study rely on ultrasound administered in the presence of microbubbles followed by radiation to induce large amounts of cell death. Our recent observations indicate that such treatment enhances the effects of radiation on endothelial cells inducing apoptotic cell death which leads to vascular collapse and secondary tumour cell death due to a mechanism of ischemia and are described elsewhere (Czarnota et al. 2009*)*.

CONCLUSIONS

The ultimate goal of this research is to apply advanced ultrasound imaging techniques to measure tumour response in patients and to provide clinically important information at a much earlier time than the current standard. This study establishes proof of principle in a previously untested tumour model, prostate cancer, and with a novel combined treatment approach. The *in vivo* model here demonstrates significant and reproducible changes in both midband fit and 0-MHz parameters as high as +5.23 dBr and +6.32 dBr, respectively, in maximally treated tumours which correlate with histopathologic measures of cell death. The current experiments also support the growing body of research suggesting that quantitative ultrasound techniques have the potential to detect and predict tumour response. Early clinical studies are in progress to assess the feasibility of applying this approach to locally advanced breast cancer and prostate cancer.

Acknowledgments—This research was supported by the Canadian Cancer Society Research Institute in addition to the Terry Fox Foundation and Sunnybrook Health Sciences Centre. JL received support from the American Institute of Ultrasound in Medicine. GJC was supported through a Cancer Care Ontario Research Chair in Imaging and Experimental Therapeutics. MCK was supported through a Tier II Canada Research Chair in Biomedical Applications of Ultrasound.

REFERENCES

Al-Mahrouki A, Karshafian R, Giles A, Wong E, Iradji S, Czarnota G. Microbubble and ultrasound induction of gene expression associated with novel radiation-enhancing therapy. Presented at AIUM Annual Meeting, New York, NY, May, 2011.

Banihashemi B, Vlad R, Debeljevic B, Giles A, Kolios MC, Czarnota GJ. Ultrasound imaging of apoptosis in tumour response: Novel preclinical monitoring of photodynamic therapy effects. Cancer Res 2008;68:8590–8596.

Bigelow TA, Oelze ML, O'Brien WD Jr. Estimation of total attenuation and scatterer size from backscattered ultrasound waveforms. J Acoust Soc Am 2005;117(3 Pt 1):1431–1439.

Bridal SL, Wallace KD, Trousil RL, Wickline SA, Miller JG. Frequency dependence of acoustic backscatter from 5 to 65 MHz ($0.06 < ka < 4.0$) of polystyrene beads in agarose. J Acoust Soc Am 1996;100: 1841–1848.

Brindle K. New approaches for imaging tumour responses to treatment. Nat rev Cancer 2008;8:94–107.

Bromfield GP, Meng A, Warde P, Bristow RG. Cell death in irradiated prostate epithelial cells: Role of apoptotic and clonogenic cell kill. Prostate Cancer Prostatic Dis 2003;6:73–85.

Carpenter AE, Jones TR, Lamprecht MR, Clarke C, Kang IH, Friman O, Guertin DA, Chang JH, Lindquist RA, Moffat J, Golland P, Sabatini DM. CellProfiler: Image analysis software for identifying and quantifying cell phenotypes. Genome Biol 2006;7:R100.

Czarnota GJ, Kolios MC, Vaziri H, Benchimol S, Ottensmeyer FP, Sherar MD, Hunt JW. Ultrasonic biomicroscopy of viable, dead and apoptotic cells. Ultrasound Med Biol 1997;23:961–965.

Czarnota GJ, Kolios MC. Ultrasound detection of cell death. Imaging Med 2010;2:17–28.

Czarnota GJ, Kolios MC, Abraham J, Portnoy M, Ottensmeyer FP, Hunt JW, Sherar MD. Ultrasound imaging of apoptosis: High-resolution noninvasive monitoring of programmed cell death *in vitro, in situ* and *in vivo*. Br J Cancer 1999;81:520–527.

Czarnota GJ, Karshafian R, Giles A, Al Mahrouki A. Microbubble and ultrasound enhancement of radiation-induced tumour cell death *in vivo*. Proc IEEE Int Ultrason Symp 2009.

Garcia-Barros M, Paris F, Cordon-Cardo C, Lyden D, Rafii S, Haimovitz-Friedman A, Fuks Z, Kolesnick R. Tumour response to radiotherapy regulated by endothelial cell apoptosis. Science 2003;300:1155–1159.

Hunt JW, Worthington AE, Xuan A, Kolios MC, Czarnota GJ, Sherar MD. A model based upon pseudo regular spacing of cells combined with the randomisation of the nuclei can explain the significant changes in high-frequency ultrasound signals during apoptosis. Ultrasound Med Biol 2002;28:217–226.

Karshafian R, Bevan PD, Williams R, Samac S, Burns PN. Sonoporation by ultrasound-activated microbubble contrast agents: Effect of acoustic exposure parameters on cell membrane permeability and cell viability. Ultrasound Med Biol 2009;35:847–860.

Kolios MC, Czarnota GJ, Lee M, Hunt JW, Sherar MD. Ultrasonic spectral parameter characterization of apoptosis. Ultrasound Med Biol 2002;28:589–597.

Lanka B, Jang HJ, Kim TK, Burns PN, Wilson SR. Impact of contrast-enhanced ultrasonography in a tertiary clinical practice. J Ultrasound Med 2007;26:1703–1714.

Lizzi FL, Astor M, Feleppa EJ, Shao M, Kalisz A. Statistical framework for ultrasonic spectral parameter imaging. Ultrasound Med Biol 1997;23:1371–1382.

Lizzi FL, Alam SK, Mikaelean S, Lee P, Feleppa EJ. On the statistics of ultrasonic spectral parameters. Ultrasound Med Biol 2006;32: 1671–1685.

Mulvagh SL, Rakowski H, Vannan MA, Abdelmoneim SS, Becher H, Bierig SM, Burns PN, Castello R, Coon PD, Hagen ME, Jollis JG, Kimball TR, Kitzman DW, Kronzon I, Labovitz AJ, Lang RM, Mathew J, Moir WS, Nagueh SF, Pearlman AS, Perez JE, Porter TR, Rosenbloom J, Strachan GM, Thanigaraj S, Wei K, Woo A, Yu EH, Zoghbi WA. American Society of Echocardiography Consensus Statement on the Clinical Applications of Ultrasonic Contrast Agents in Echocardiography. J Am Soc Echocardiogr 2008;21:1179–1201.

Nieder C, Wiedenmann N, Andratschke N, Molls M. Current status of angiogenesis inhibitors combined with radiation therapy. Cancer Treat Rev 2006;32:348–364.

Oelze ML, O'Brien WD Jr, Blue JP, Zachary JF. Differentiation and characterization of rat mammary fibroademonas and 4T1 mouse carcinomas using quantitative ultrasound imaging. IEEE Trans Med Imaging 2004;23:764–771.

Ranieri S, Vlad R, Debeljevic B, Giles A, Kolios MC, Czarnota GJ. High frequency ultrasound: Detection and differentiation of apoptosis and necrosis during cancer therapy. American Institute of Ultrasound in Medicine (AIUM) Annual Meeting, San Diego, USA. E-pub, 2008.

Rasband WS, ImageJ, U. S. National Institutes of Health, Bethesda, Maryland, USA. Available at: http://imagej.nih.gov/ij/, 1997–2011. Accessed June 2011.

Shung KK. Diagnostic ultrasound: Imaging and blood flow measurements. Boca Raton: CRC Press; 2005:155.

Taggart LR, Baddour RE, Giles A, Czarnota GJ, Kolios MC. Ultrasonic characterization of whole cells and isolated nuclei. Ultrasound Med Biol 2007;33:389–401.

Unger EC, Matsunaga TO, McCreery T, Schumann P, Sweitzer R, Quigley R. Therapeutic applications of microbubbles. Eur J Radiol 2002;42:160–168.

Verheij M, Bartelink H. Radiation-induced apoptosis. Cell Tissue Res 2000;301:133–142.

Vlad RM, Czarnota GJ, Giles A, Sherar MD, Hunt JW, Kolios MC. High-frequency ultrasound for monitoring changes in liver tissue during preservation. Phys Med Biol 2005;50:197–213.

Vlad RM, Alajez NM, Giles A, Kolios MC, Czarnota GJ. Quantitative ultrasound characterization of cancer radiotherapy effects *in vitro*. Int J Radiat Oncol Biol Phys 2008;72:1236–1243.

Vlad RM, Brand S, Giles A, Kolios MC, Czarnota GJ. Quantitative ultrasound characterization of responses to radiotherapy in cancer mouse models. Clin Cancer Res 2009;15:2067–2075.